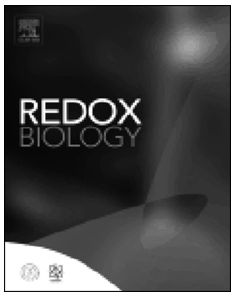

(-)-Epicatechin and NADPH oxidase inhibitors prevent bile acid-induced Caco-2 monolayer permeabilization through ERK1/2 modulation

Ziwei Wang, M. Corina Litterio, Michael Müller, David Vauzour, Patricia I. Oteiza

PII: S2213-2317(19)31145-0

DOI: https://doi.org/10.1016/j.redox.2019.101360

Reference: REDOX 101360

To appear in: *Redox Biology*

Received Date: 18 September 2019

Revised Date: 19 October 2019

Accepted Date: 21 October 2019

Please cite this article as: Z. Wang, M.C. Litterio, M. Müller, D. Vauzour, P.I. Oteiza, (-)-Epicatechin and NADPH oxidase inhibitors prevent bile acid-induced Caco-2 monolayer permeabilization through ERK1/2 modulation, *Redox Biology* (2019), doi: https://doi.org/10.1016/j.redox.2019.101360.

Graphical abstract

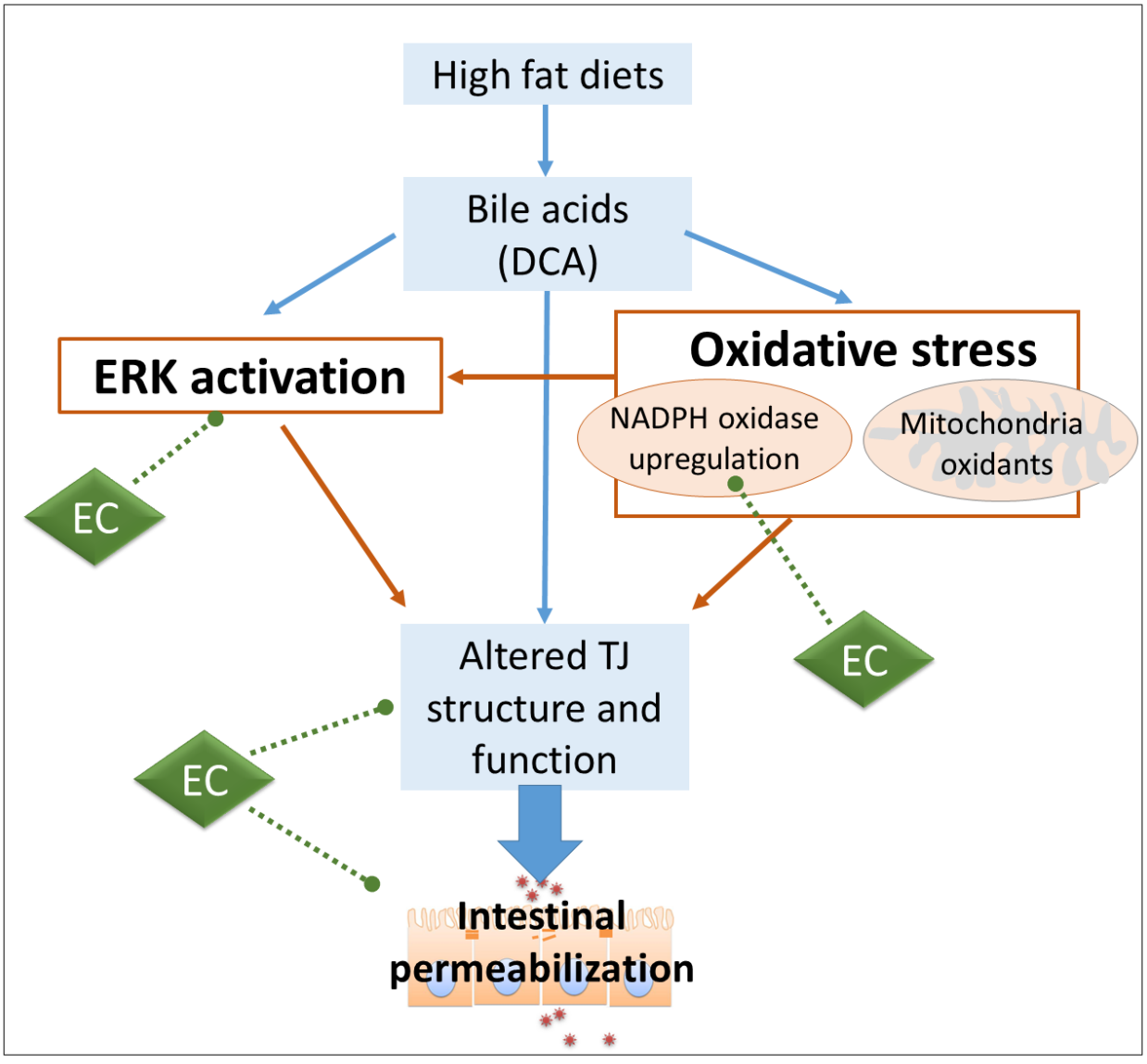

(-)-Epicatechin and NADPH oxidase inhibitors prevent bile acid-induced Caco-2 monolayer permeabilization through ERK1/2 modulation.

Ziwei Wang[a], M. Corina Litterio[a,b], Michael Müller[c], David Vauzour[c] and Patricia I. Oteiza[a,#]

[a]Departments of Nutrition and Environmental Toxicology, University of California, Davis, CA, USA

[b]Instituto de Bioquímica y Medicina Molecular (IBIMOL), CONICET-Universidad de Buenos Aires, Buenos Aires, Argentina

[c]Norwich Medical School, Biomedical Research Centre, University of East Anglia, Norwich, UK

[#]Corresponding author

Dr. Patricia I. Oteiza
Department of Nutrition
University of California, Davis
One Shields Av. Davis, CA 95616, USA.
Phone: 530-754-6074, Fax: 530-752-8966, Email: poteiza@ucdavis.edu

Running title: Epicatechin protects the intestinal barrier

Abbreviations: DCA, deoxycholic acid; DCFDA, 5-(and-6)-carboxy-2'7'-dichlorodihydrofluorescein diacetate; DHE, dihydroethidium; EC, (-)-epicatechin; EGF, epidermal growth factor; EGFR, EGF receptor; ERK, extracellular signal-regulated kinase; GI, gastrointestinal; MLC, myosin light chain; MLCK, MLC kinase; MEM, minimum essential medium; MMP, matrix metalloproteinase; NOX, NADPH oxidase; ROS, reactive oxygen species; TJ, tight junction

Keywords
Bile acids, deoxycholic acid, epicatechin, intestinal permeability, high fat

ABSTRACT

Secondary bile acids promote gastrointestinal (GI) tract permeabilization both *in vivo and in vitro*. Consumption of high fat diet s increases bile acid levels in the GI tract which can contribute to intestinal permeabilization and consequent local and systemic inflammation. This work investigated the mechanisms involved in bile acid (deoxycholic acid (DCA))-induced intestinal epithelial cell monolayer permeabilization and the preventive capacity of (-)-epicatechin (EC). While EC prevented high fat diet-induced intestinal permeabilization in mice, it did not mitigate the associated increase in fecal/cecal total and individual bile acids. *In vitro*, using differentiated Caco-2 cells as a model of epithelial barrier, EC and other NADPH oxidase inhibitors (VAS-2870 and apocynin) mitigated DCA-induced Caco-2 monolayer permeabilization. While EC inhibited DCA-mediated increase in cell oxidants, it did not prevent DCA-induced mitochondrial oxidant production. Prevention of DCA-induced ERK1/2 activation with EC, VAS-2870, apocynin and the MEK inhibitor U0126, also prevented monolayer permeabilization, stressing the key involvement of ERK1/2 in this process and its redox regulation. Downstream, DCA promoted myosin light chain (MLC) phosphorylation which was related to MLC phosphatase (MLCP) inhibition by ERK1/2. DCA also decreased the levels of the tight junction proteins ZO-1 and occludin, which can be related to MMP-2 activation and consequent ZO-1 and occludin degradation. Both events were prevented by EC, NADPH oxidase and ERK1/2 inhibitors. Thus, DCA-induced Caco-2 monolayer permeabilization occurs mainly secondary to a redox-regulated ERK1/2 activation and downstream disruption of TJ structure and dynamic. EC's capacity to mitigate *in vivo* the gastrointestinal

permeabilization caused by consumption of high-fat diets can be in part related to its capacity to inhibit bile-induced NADPH oxidase and ERK1/2 activation.

Introduction

Consumption of Western type diets high in saturated fats has deleterious consequences on the gastrointestinal (GI) tract. They include, among others, a higher risk for colorectal cancer [1-3], altered intestinal immunity [4], inflammation [5], and intestinal permeabilization [5-7]. In fact, an increased intestinal permeability and the associated local and systemic inflammation can underlie several of high fat diet- and obesity-associated morbidities [8, 9].

The permeability of the GI tract is determined by the tight junction (TJ), which connect a single layer of epithelial cells [10]. Intercellular TJs are a complex of proteins including both integral (e.g. occludin, claudins) and intracellular (e.g. ZO-1, ZO-2) proteins that are linked to an actomyosin ring. TJs selectively allow the passage of water and ions and restricts the paracellular transport of larger molecules. The unrestricted intestinal passage of large molecules (e.g. pathogens, luminal food and microbial toxins) can have direct systemic effects, activating the GI immune system leading to local inflammation and the systemic release of proinflammatory cytokines. Accordingly, a loss of intestinal barrier integrity/function has been observed in several human pathologies [5].

Select bile acids increase GI permeability both *in vivo* and in *in vitro* models. Thus, the intestinal permeabilization observed in rats fed a high-fat diet was found to be related to both the dietary fat itself and the associated increased intestinal levels of bile acids [11]. Deoxycholic acid (DCA), a hydrophobic secondary bile acid, promotes the permeabilization of Caco-2 cell monolayers [12]. DCA affects the physical properties of cell membrane domains [13], which is associated to the activation of cell signals that regulate TJ permeability. In intestinal epithelial cells

DCA causes the activation of the epidermal growth factor (EGF) receptor (EGFR) [13, 14], and downstream the ERK1/2 signaling pathway [15]. Together with transcription factor NF-κB, ERK1/2 upregulates myosin light chain (MLC) kinase (MLCK), a central physiological modulator of TJ permeability [10, 16, 17]. Bile acids also downregulate TJ proteins expression, which could contribute to DCA-mediated barrier permeabilization [12]. Overall, the increased bile acid production and luminal content required for fat absorption could explain the increased permeabilization of the GI tract observed with consumption of high-fat diets.

Diet has a major role in the development and progression of GI-associated pathologies. Among dietary factors, flavonoid-rich foods can exert GI protective and trophic effects through different mechanisms [18]. In particular, the flavan-3-ol (-)-epicatechin (EC) prevents inflammation- and high fat diet-induced intestinal permeabilization both *in vitro* and *in vivo* [19, 20]. *In vitro*, EC prevents tumor necrosis alpha (TNFα)-induced permeabilization of Caco-2 cell monolayers through the inhibition of NADPH oxidase, leading to a decrease in superoxide production, and inactivation of the transcription factor NF-κB [19]. In mice fed a high-fat diet, supplementation with EC prevented the increased GI permeability and the associated endotoxemia [20].

An increase in luminal bile acids can in part underlie the increased intestinal permeabilization associated with the consumption of diets rich in fat content, contributing to the associated co-morbidities. On the other hand, a diet rich in select bioactives (e.g. EC) could mitigate intestinal permeabilization by inhibiting bile-acid mediated barrier damage. This work investigated the mechanisms involved in bile acid (deoxycholic acid (DCA))-induced intestinal epithelial cell monolayer permeabilization and the preventive capacity of EC. We initially studied if

the capacity of EC to prevent high fat diet-induced intestinal permeabilization in mice could occur through the modulation of bile acid metabolism. Subsequently, and using Caco-2 cell monolayers as a model of intestinal barrier, we investigated the potential capacity of EC to prevent bile direct effects on the epithelium. The ERK1/2 signaling pathway emerges as a central mechanism in DCA-induced monolayer permeabilization. The protective action of EC is in part mediated by its capacity to inhibit NADPH oxidase, oxidant production, and downstream ERK1/2 activation.

Materials and methods

Materials

Caco-2 cells were from the American Type Culture Collection (ATCC, Rockville, MA). Cell culture media and reagents, 5-(and-6)-carboxy-2'7'-dichlorodihydrofluorescein diacetate (DCFDA), MitoSOX Red mitochondrial superoxide indicator (M36008), and primary antibodies for ZO-1 (#339100), occludin (#331500), claudin-1 (#717800), and claudin-2 (#325600) were from Invitrogen/Life Technologies (Grand Island, NY). U0126 (#9903) and primary antibodies for phospho-p44/42 ERK1/2 (Thr202/Tyr204) (#4370), p44/42 ERK1/2 (#4695), phospho-p65 (Ser536) (#3033), p65 (#8242), phospho-MLC 2 (Ser19) (#3671), MLC 2 (#8505), phospho-MYPT1 (Thr696) (#5163); MYPT1 (#8574), phospho-EGFR (Tyr1068) (#3777), EGFR (#4267), and β-actin (#12620) were from Cell Signaling Technology (Danvers, MA). DCA, EC, apocynin, VAS-2870, FITC-dextran, and dihydroethidium (DHE) were from Sigma Chem. Co. (St. Louis, MO). The Amplex® Red Hydrogen Peroxide/Peroxidase Assay Kit was from Thermo Fisher Scientific (Waltham, MA).

Animals and animal care

All procedures conducted during this study were in agreement with standards for the care of laboratory animals as outlined in the NIH Guide for the Care and Use of Laboratory Animals. All procedures were administered under the auspices of the Animal Resource Services of the University of California, Davis. Experimental protocols were approved before implementation by the University of California, Davis Animal Use and Care Administrative Advisory Committee.

Healthy male C57BL/6J mice (20-25 g) (7 mice/group) were divided into 2-3 mice per cage, housed at 21-22°C and 53-55% humidity on a 12-hour light-dark cycle. They were fed for 15 weeks either: A- a diet containing approximately 10% total calories from fat (Control) (TD.06416, Harlan Laboratories, Madison, WI), B- a diet containing approximately 60% total calories from fat (lard) (HF) (TD.06414, Harlan Laboratories, Madison, WI), and C- the high fat diet supplemented with 20 mg EC/kg body weight (HFE) as previously described [20]. The EC-containing diet was prepared every two weeks to account for changes in body weight and food intake, and to prevent potential EC degradation. All diets were stored at -20°C until use. Details on metabolic parameters and *in vivo* evaluation of intestinal permeability for this animal study have been previously published [20]. After 15 weeks on the dietary treatments, mice were euthanized by cervical dislocation. The cecum content and feces were collected and stored at -80°C until analysis for bile acid content.

Determination of total and individual bile acids

For total bile acid content determination, feces were weighed and dried in an oven at 37˚C for 24 h. Samples were subsequently powdered using a mortar, and bile acids were hydrolyzed under alkaline conditions at 220˚C. Subsequently, samples were neutralized with 12N HCl, followed by three extractions in diethyl ether, as previously described [21, 22]. Total bile acids were measured using a 3-α hydroxysteroid dehydrogenase assay kit (Crystal Chem, Inc., IL, USA).

For individual bile acid analysis, mice cecum samples (20 mg) were homogenized in 1 ml of 70% (v/v) methanol containing 25 µl of 40 µg/ml d4 (deuterated)-DCA for 30 sec at 6,000 rpm on a Precellys homogenizer (Bertin Technologies, UK). The slurry was then centrifuged at 1,000 x g at 4°C and the supernatant transferred to a new tube and added with 25 µl of 40 µg/ml d4-chenodeoxycholic acid. Samples were concentrated by centrifugal evaporation at 50°C for 70 min to almost dryness using a SpeedVac™ concentrator, and then brought to 1 ml volume with 5% (v/v) methanol and added with 25 µl of 40 µg/ml d4-cholic acid. The reconstituted samples were passed through a hydrophilic-lipophilic balance clean-up cartridge (Waters Oasis Prime HLB, 1 ml, 30 mg), washed with 1 ml of 5% (v/v) methanol and eluted in 500 µl methanol added with 25 µl of 40 µg/ml d4-glycholic acid and d4-lithocholic acid. Of the internal standards added, d4-glycholic acid was the primary reference internal standard, with the others monitored as checks in the extraction procedure. The final sample was submitted for analysis by LC-MS/MS using an Agilent 1260 binary HPLC coupled to an AB Sciex 4000 QTrap triple quadrupole mass spectrometer. HPLC was carried out using a binary gradient of solvent A (water + 5 mM ammonium acetate + 0.012% (v/v) formic acid) and solvent B (methanol + 5 mM ammonium acetate + 0.012% (v/v) formic acid) at a constant flow rate of 600 µl/min. Separation was achieved using a Supelco Ascentis Express C18 150 x 4.6, 2.7µm column maintained at 40°C. The mass spectrometer was operated in

electrospray negative mode with capillary voltage of 4500V at 550°C. Instrument specific gas flow rates were 25 ml/min curtain gas, GS1: 40 ml/min and GS2: 50 ml/min. Mass fragmentation was monitored in MRM mode. Quantification was applied using Analyst 1.6.2 software to integrate detected peak areas relative to the deuterated internal standards.

Cell culture and incubations

Caco-2 cells were cultured at 37^{o}C and 5% (v/v) CO_2 atmosphere in minimum essential medium (MEM) supplemented with 10% (v/v) fetal bovine serum and antibiotics (50 U/ml penicillin, and 50 µg/ml streptomycin). For the experiments, cells seeded in semipermeable membranes or in regular dishes were differentiated for 18-21 or 9-12 days, respectively, after confluence. The cell culture medium was replaced every 3 days. Cells were then incubated in the absence or the presence of 100 µM DCA, with or without EC (1-10 µM), 1 µM apocynin, 1 µM VAS-2870, and 10 µM U0126, for the time period indicated for each experiment. After the corresponding incubations, the medium was collected for matrix metalloproteinase (MMP) determination, and cells collected and processed accordingly for the different determinations

Cell viability

Cell viability was evaluated using the MTT (3-[4,5-dimethylthiazol-2-yl]-2,5 diphenyl tetrazolium bromide) assay which is based on the conversion of MTT into formazan crystals by living cells. Cells were treated with DCA and/or EC as described above, and at the end of the

incubation cells were added with a 0.5 mg/ml MTT solution in PBS. After 2 h of incubation at 37 °C, the reaction was stopped by addition of DMSO, and plates were incubated overnight. Absorbance (λ 570-690 nm) was measured using a BioTek Synergy H1 plate reader (BioTek Instruments, Winooski, VT) and expressed as percentage of untreated (control) cell values.

Transport of fluorescein isothiocyanate-dextran (FITC-dextran)

Cells were differentiated into polarized monolayers by culture on transwell inserts (12 mm, 0.4 μm pore polyester membranes) placed in 24-well plates at a seeding density of 0.3 x 10^6 cells/transwell. The volume of medium added to the upper and lower compartments was 400 μl and 600 μl, respectively. The paracellular transport through Caco-2 cell monolayers was determined by measuring the apical-to-basolateral clearance of FITC-dextran (4 kDa). DCA (100 μM) and EC (1-10 μM), the NADPH oxidase inhibitors apocynin and VAS-2870 (1 μM) or U0126 (10 μM) were added to the apical compartment. FITC-dextran was subsequently added to this compartment (100 μg/ml final concentration), and 100 μl of the medium in the lower compartment were collected every hour for 4 h. Aliquots were diluted with 100 μl of MEM without phenol red, and the fluorescence was measured at λexc: 485 nm and λem: 530 nm in a plate reader (Biotek Synergy H1 plate reader, BioTek Instruments, Winooski, VT). The FITC-dextran clearance (CL_{FITC}) was calculated using the equation fFITC/(FFITC/A), where fFITC is flux of FITC-dextran (in fluorescence units/h); FFITC, the fluorescence of FITC-dextran in the upper compartment at zero time (in fluorescence units per nl); and A, the surface area of the membrane

(1 cm^2). Arbitrary units (AU) were calculated based on the CL_{FITC} value for the non-added (control) cells which showed a mean CL_{FITC}=75 nl/h/cm^2.

Cell oxidant levels

Cell oxidant levels were estimated using the probes DCFDA, DHE and Amplex® Red. DCFDA and DHE enter cells, and when oxidized are converted into fluorescent compounds. Caco-2 cells were grown and differentiated in 96 well plates. Cells were incubated for 0.5-4 h in the absence or presence of 100 µM DCA with or without the addition of 5 µM EC. At the corresponding times, cells were added with 20 µM DCFDA or 10 µM DHE, and after 30 min incubation the medium was removed, cells rinsed with PBS, and fluorescence measured, for oxidized DCFDA at λexc: 485 nm; λem: 535 nm, and for oxidized DHE at λexc: 485 nm; λem: 535 nm. To normalize for the number of cells, DCFDA and Amplex® Red fluorescence was referred to the DNA content measured with propidium iodide as previously described [19], and DHE fluorescence was referred to protein content. H_2O_2 released to the medium was measured at the corresponding time points with the Amplex® Red Hydrogen Peroxide/Peroxidase Assay Kit following the manufacturer's protocol.

Mitochondria oxidant production

Mitochondria oxidants production was determined using the MitoSOX Red reagent, which is oxidized in the mitochondria mainly by superoxide, and exhibits red fluorescence. Caco-2 cells were grown and differentiated in 24 well plates. Cells were incubated for 0.5-4 h in the absence or

presence of 100 μM DCA with or without the addition of 5 μM EC. Cells were dissociated by treatment with trypsin, washed once with PBS and the pellet resuspended in 0.4 ml PBS containing 5 μM MitoSOX Red (from a 5 mM reagent stock solution prepared in DMSO). Cells were subsequently incubated for 30 min at room temperature, protected from light. Appropriate controls were prepared: a positive control incubated with Antimycin A (20 μM), known to produce a burst of superoxide (and therefore an increase in MitoSOX fluorescence), and a negative control of cells incubated in the absence of MitoSOX. Cell fluorescence was measured in a FACSCanto II Flow Cytometer (BD Biosciences, San Jose, CA). Data were acquired by CellQuest Software (BD Biosciences, San Jose, CA) and analyzed using FlowJo (BD Biosciences, San Jose, CA).

RNA isolation and real-time PCR (RT-PCR)

For quantitative RT-PCR studies, RNA was extracted from cells using TRIzol reagent (Invitrogen, Carlsbad, CA). cDNA was generated using high-capacity cDNA Reverse Transcriptase (Applied Biosystems, Grand Island, NY). Expression of NOX1, NOX4, MLCK and actin was assessed by quantitative real-time PCR (iCycler, Bio-Rad, Hercules, CA) with the following primers:

Primer NOX1 Forward: 5'-GTACAAATTCCAGTGTGCAGACCAC-3'
Primer NOX1 Reverse: 5'-GTACAAATTCCAGTGTGCAGACCAC-3'

Primer NOX4 Forward: 5’-CTCAGCGGAATCAATCAGCTGTG-3’
Primer NOX4 Reverse: 5’-AGAGGAACACGACAATCAGCCTTAG-3’

Primer MLCK Forward: 5'-GAGGTGCTTCAGAATGAGGACG -3'
Primer MLCK Reverse: 5'- GCATCAGTGACACCTGGCAACT -3'

Primer β-Actin Forward: 5'-TCATGAAGTGTGACGTGGACATCCGC-3'
Primer β-Actin Reverse: 5'-CCTAGAAGCATTTGCGGTGCACGATG-3'

Western blot analysis

Total fractions were prepared as previously described [15]. Protein concentration was measured [23] and aliquots containing 25-100 μg protein were separated by reducing 10% (w/v) polyacrylamide gel electrophoresis and electroblotted to PVDF membranes. Colored (Biorad Laboratories, Hercules, CA) and biotinylated (Cell Signaling Technologies, Danvers MA) molecular weight standards were ran simultaneously. Membranes were blotted for 1 h in 5% (w/v) non-fat milk, incubated overnight in the presence of the corresponding antibodies (1:1,000 dilution) in 5% (w/v) bovine serum albumin in TBS buffer (50 mM Tris, 150 mM NaCl, pH 7.6), containing 0.1% (v/v) Tween-20. After incubation for 90 min at room temperature in the presence of the secondary antibody (HRP-conjugated) (1:10,000 dilution) the conjugates were visualized by chemiluminescence detection in a Phosphoimager 840 (Amersham Pharmacia Biotech. Inc., Piscataway, NJ).

Detection of matrix metalloproteinases by gelatin zymography

Analysis of MMPs gelatinolytic activity was performed using 7.5% (w/v) polyacrylamide gels impregnated with 0.1% (w/v) gelatin. After 2 h incubation in the corresponding conditions, same

volumes of medium were collected from all wells, samples were centrifuged at 800 x g for 8 min to eliminate cell debris, and concentrated 7X using a Vacufuge concentrator (Eppendorf, Germany). Non-reducing sample buffer was added to 75 µl of the concentrated medium, and proteins were separated by SDS-PAGE. Gels were washed 3 times in washing buffer (2.5% (v/v) Triton X-100, 50 mM Tris-HCl pH 7.5, 5 mM $CaCl_2$, 1 µM $ZnCl_2$) for 20 min at room temperature to remove the SDS. Gels were subsequently equilibrated with incubation buffer (1% (v/v) Triton X-100, 50 mM Tris-HCl pH 7.5, 5 mM $CaCl_2$, 1 µM $ZnCl_2$) for 10 min at 37 °C, which was subsequently replaced with fresh buffer, and gels incubated for 24 h at 37 °C. Gels were stained with Coomassie Brilliant Blue R-250 (Biorad Laboratories, Hercules, CA) overnight, and destained in a solution containing 10% (v/v) acetic acid and 40% (v/v) methanol, until the gelatinase activity was clearly seen. Bands were visualized in MyECL Imager (Thermo Scientific, New York, NY, USA).

Statistical analysis

All values are shown as means ± standard error of the means (SEM). Data were analyzed by one-way analysis of variance (ANOVA) using GraphPad Prism 7.0 (GraphPad Software, San Diego, CA, USA). Fisher least significance difference test was used to examine differences between group means. A p value < 0.05 was considered statistically significant.

Results

Bile acid profiles in mice fed a high-fat diet: effects of EC

We previously observed that EC prevents high-fat diet-triggered intestinal permeabilization [20]. In the same group of C57BL/6J mice, consumption of the high-fat diet for 14 weeks led to a significant ($p < 0.05$) increase in total fecal bile acids compared to levels found in mice fed the control diet (**Fig. 1A**). Dietary supplementation with EC (20 mg/kg body weight) did not affect high fat diet -mediated increase in total fecal bile acid levels (**Fig. 1A**). Cecal unconjugated and conjugated bile acids were subsequently characterized by HPLC-MS in MRM mode (**Fig. 1 B-E**). Compared to controls, consumption of the high-fat diet caused significantly higher levels of cecal β-muricholic acid, cholic acid, deoxycholic acid, taurochenodeoxycholic acid, glycholic acid, taurodeoxycholic acid and glycohyodeoxycholic acid. EC supplementation did not prevent those increases (**Fig. 1 B-E**).

EC prevents DCA-induced Caco-2 cell monolayer permeabilization

We next investigated if EC could inhibit DCA-induced monolayer permeabilization of human Caco-2 cells differentiated into intestinal epithelial cells. Under the experimental conditions used (100 µM DCA and/or 1-10 µM EC) and upon 4 h incubation, neither DCA nor EC affected cell viability (**Fig. 2A**). Changes in monolayer permeability were evaluated by measuring the paracellular transport of the fluorescent probe FITC-dextran (**Fig. 2B-D**). DCA (100 µM) caused a time (0-4 h)-dependent increase in FITC-dextran transport from the upper to the lower chamber (**Fig. 2B**). EC (1-10 µM) inhibited DCA-mediated increase in FITC-dextran clearance at 2 h (**Fig. 2C**) and 3 h (data not shown). After 4 h incubation, 1 µM EC had no effects while 5 and 10 µM EC inhibited DCA-induced increase in FITC-dextran paracellular transport (**Fig. 2D**).

DCA increases NADPH oxidase expression and ROS production: effects of EC

We previously observed that DCA-induced Caco-2 monolayer permeabilization was associated with increases in reactive oxygen species (ROS) production [12, 15]. EC has been shown to both inhibit NADPH oxidase activation and prevent NOX1/NOX4 overexpression [20]. Thus, we next investigated if the capacity of EC to prevent DCA-induced permeabilization could be associated with the modulation of ROS production, characterizing the two main ROS cellular sources, NADPH oxidase and mitochondria.

NOX1 and NOX4 are the main NADPH oxidases present in Caco-2 cells (data not shown). DCA did not affect NOX1 expression within the studied period (0.5-4 h), while a significant increase in NOX4 mRNA levels was observed after 3 and 4 h incubation with DCA (**Fig. 3A**). EC (5 µM) prevented the increase in NOX4 expression after 3 h incubation with DCA (**Fig. 3B**). Given that EC has been shown to also inhibit NADPH activity we next assessed the capacity of EC to prevent DCA-mediated increase in cellular ROS. This was assessed using three different probes; Amplex® Red, DCFDA and DHE. While Amplex® Red fluorescence increase only reached significance after 4 h incubation with DCA, DCA-induced DCFDA fluorescence increase was significant at 2 and 4 h and DHE fluorescence increase was significant at 0.5, 1 and 4h (**Fig. 3C**). EC prevented DCA-mediated increases in oxidant production at all time points for the three probes used (data not shown). **Fig. 3D** shows EC inhibition of ROS increase at the corresponding time points of highest DCA effect, i.e. 4 h for Amplex® Red and DCFDA fluorescence (12 and 75% higher in DCA-treated than in control cells, respectively) and 30 min for DHE fluorescence (45% higher in DCA-treated than in control cells) (**Fig. 3D**).

DCA increased mitochondrial ROS production as evaluated by reaction with MitoSOX and subsequent FACS (**Fig. 3 E-G**). DCA caused a significant increase in mitochondrial ROS production starting at 30 min incubation with DCA, which remained high for the following 3.5 h (**Fig. 3F**). After 2 h incubation with DCA, MitoSOX fluorescence increased to 2.1-fold over control values, and EC (5 µM) showed no preventive effects (**Fig. 3G**).

The ERK1/2 pathway is involved in DCA-induced Caco-2 cell monolayer permeabilization: inhibition by EC and other NADPH oxidase inhibitors

The redox-sensitive signals NF-κB and ERK1/2 are the main pathways controlling intestinal epithelium permeability. We next investigated the effects of DCA on the activation of NF-κB and ERK1/2 by measuring the phosphorylation of p65 (Ser536) and ERK1/2 (Thr202/Tyr204) by Western blot. p65 phosphorylation levels were not affected by treatment with 100 µM DCA along a 4 h incubation period (**Fig. 4A**). On the other hand, ERK1/2 phosphorylation significantly increased (34 to 84%) within 1 to 4 h incubation with DCA, when compared to basal levels. Upstream ERK1/2, DCA increased (100% over control values) the activating phosphorylation (Tyr1068) of the EGFR, which was prevented by EC (**Fig. 4B**). After 2 h incubation, EC (5 µM), apocynin (1µM) and VAS-2870 (1µM), fully prevented DCA-mediated increase of ERK1/2 phosphorylation (**Fig. 4B,C**).

To understand the role of ERK1/2 on DCA-induced Caco-2 monolayer permeabilization we inhibited the pathway with the MEK inhibitor U0126. At 10 µM concentration, U0126 not only fully inhibited DCA-mediated increase in ERK1/2 phosphorylation, but values were 64% lower than

basal levels (**Fig. 4C**). Stressing a central role of ERK1/2 in the permeabilization induced by DCA, U0126 also prevented the increase in FITC-dextran clearance (**Fig. 4D**). The NADPH oxidase inhibitors Apocynin and VAS-2870 were also effective inhibiting DCA-mediated increase in ERK1/2 phosphorylation and permeabilization of the monolayer (**Fig. 4C,D**).

Effects of DCA on MLC phosphorylation: role of EC

Phosphorylation of MLC is a central mechanism involved in TJ opening and barrier permeabilization. After 2 h incubation, DCA caused a 30% increase in the levels of MLC phosphorylation at Ser19. EC (5 μM), NADPH oxidase inhibitors (1 μM), and U0126 (10 μM) fully inhibited this increase (**Fig. 5A**). MLC is phosphorylated in Thr19/Ser19 by MLCK and dephosphorylated by MLC phosphatase. To evaluate the potential upregulation of MLCK by DCA, the mRNA levels of the kinase were measured by RT-PCR. DCA cause a time-dependent decrease in MLCK mRNA levels (**Fig. 5B**). After 2 h incubation, MLCK mRNA levels were similar among the DCA-treated cells in both the absence and the presence of the inhibitors (**Fig. 5C**). On the other hand, DCA caused a significant increase (27%) in the phosphorylation levels of the MLC phosphatase regulatory subunit MYPT1 at Thr696 (**Fig. 5D**). This increase was prevented by EC (5 μM), NADPH oxidase inhibitors (1 μM), and U0126 (10 μM).

DCA promotes the downregulation of tight junction proteins

The TJ is composed by several proteins including ZO-1, occludin and claudins. To assess if DCA could act permeabilizing the Caco-2 monolayer by affecting the expression of TJ proteins, the protein content of ZO-1, occludin and claudin 1 and 2 were measured by Western blot. DCA

promoted a time-dependent decrease in ZO-1 and occludin protein levels, while not affecting those of claudins 1 and 2 (**Fig. 6A**). After 2 h incubation with DCA (100 μM), ZO-1 and occludin levels in total cell homogenates were 24 and 25% lower than in control cells, and this was prevented by co-incubation with EC (5 μM), apocynin (1 μM) and VAS-2870 (1 μM) (**Fig. 6B,C**). U0126 (10 μM) fully prevented the DCA-induced decreased expression of ZO-1, with a trend ($p= 0.06$) inhibiting DCA-mediated occludin decrease.

Metalloproteinases can degrade TJ proteins. Thus, MMP-2 activity was next measured in the cell culture medium by zymography. DCA caused a 2.1-fold increase in MMP-2 activity over control values (**Fig. 6D**). EC (5 μM), NADPH oxidase inhibitors (1 μM), and U0126 (10 μM) fully inhibited DCA-mediated MMP-2 activation.

Discussion

The capacity of EC to mitigate high fat diet-induced intestinal permeabilization in mice is not due to changes in bile acid metabolism, but it can be in part attributed to the prevention of bile (DCA)-induced barrier damage. DCA-induced Caco-2 cell monolayer permeabilization occurred secondary to NADPH oxidase and ERK1/2 activation. Permeabilization was paralleled by increased phosphorylation of MLC due to the inhibition of the MLC phosphatase. DCA also decreased the expression of the TJ proteins ZO-1 and occludin, which can be related to their degradation by MMP-2. Stressing a central role for NADPH oxidase in DCA-induced permeabilization, EC and other NADPH oxidase inhibitors prevented DCA-mediated ERK1/2 activation and the downstream events. Thus, the observed capacity of EC to inhibit intestinal

permeabilization in high fat-fed mice can be in part due to the inhibition of bile acid-induced alterations in TJ structure/dynamics.

Excess levels of select bile acids could explain the increased intestinal permeability associated to the consumption of high-fat diets [11, 20, 24]. The microbiota can contribute to this adverse effect given that it undergoes major changes upon chronic high fat consumption, and its central role in bile acid metabolism [25]. Thus, the microbiota deconjugate and dehydroxylate bile acids produced in the liver and secreted into the intestinal lumen, to generate unconjugated and secondary bile acids. While high-fat diet consumption caused major changes in mouse fecal bile acid profiles, EC supplementation did not affect neither total bile acid levels nor the individual types of bile acids. In agreement with a lack of effect of EC on unconjugated and secondary bile acids content, EC supplementation did not modify the altered microbiota profiles associated to the consumption of a high-fat diet [20]. On the other hand, the protective actions of EC on high-fat diet-induced GI loss of barrier function in mice [20], could be due to EC capacity to mitigate bile-induced intestinal monolayer permeabilization.

GI tract permeabilization can cause an increased paracellular transport of bacterial endotoxins, which trigger local and systemic inflammation, contributing to the development of pathologies, including insulin resistance, type 2 diabetes and cardiovascular diseases [6, 26, 27]. The consumption of a high-fat diet *per se*, rather than the associated obesity, have been proposed to trigger intestinal permeabilization in rats [11]. In fact, the bile juice isolated from rats fed a high-fat diet, as well as individual bile acids, promote permeabilization of Caco-2 cell monolayers [11, 19]. We observed that bile acids found at largest amounts in the cecum from high fat-fed mice are muricholic acids, cholic, and DCA. Among them, and also present in humans, DCA causes

permeabilization of intestinal monolayers [12] and is a major player in pathologies associated to consumption of high-fat diets and obesity [28].

In agreement with previous evidence [12], DCA caused the permeabilization of Caco-2 cells differentiated into a monolayer of intestinal epithelial cells, and EC prevented it. It is important to consider that the use of Caco-2 cell monolayers as a model of intestinal epithelium has limitations [29]. Among others, the Caco-2 cell population is heterogeneous, the monolayer does not involve interactions of epithelial cells with other cell types, and the model lacks a mucus layer. However, the validity of the model for our study is supported by current and previous observations on the capacity of EC to protect Caco-2 monolayers from permeabilization [19, 20], which are in accordance with the GI barrier protective effects exerted by dietary EC in high fat-fed mice [20].

EC and the NADPH oxidase inhibitors apocynin and VAS-2870 inhibited DCA-mediated increase in paracellular transport. We previously observed that the NADPH oxidase inhibitors apocynin and diphenyleneiodonium inhibited DCA-stimulated oxidant production in Caco-2 cells [12]. Accordingly, we now observed that DCA increased NOX4 expression and cell oxidant levels, which were both prevented by EC. Consistently, EC prevented high-fat diet-induced intestinal permeabilization and NADPH oxidase upregulation in mice [20]. EC, which has a structural similarity to apocynin, also directly inhibits NADPH oxidase activity in vascular endothelial cells [30], and in Caco-2 cells [19, 20]. On the other hand, while DCA increased mitochondrial ROS production, EC had no preventive effects. Thus, the above findings stress a relevant role for NADPH oxidase in DCA-mediated epithelial monolayer permeabilization, and this enzyme as a target of EC in the protection of GI barrier function.

Both NF-κB and ERK1/2 are major players in the regulation of TJ structure and dynamics. Under the current experimental conditions, 100 µM DCA did not affect NF-κB but promoted the activation of ERK1/2 in Caco-2 cells. ERK1/2 activation by DCA was previously described in hepatocytes [31, 32] and intestinal cells [15, 33]. This activation can be triggered by the interactions of DCA with the cell membrane, promotion of membrane physical alterations, and the associated activation of membrane proteins, i.e. the EGFR and cell membrane NADPH oxidases [12, 13, 15, 19, 32, 34]. In fact, we observed that DCA activated the EGFR and downstream the ERK1/2 pathway. Our findings that EC, VAS-2870, apocynin and the MEK inhibitor U0126 inhibit both ERK1/2 activation and Caco-2 monolayer permeabilization establishes a causal link between NADPH oxidase and ERK1/2 activation in DCA-induced increase in monolayer paracellular transport.

Phosphorylation of MLC is a required step in the physiological opening of the TJ and is regulated by its phosphorylation by MLCK and dephosphorylation by MLC phosphatase. DCA increased MLC phosphorylation that was inhibited by EC and by NADPH oxidase and ERK1/2 inhibitors. ERK1/2 modulates MLCK expression by phosphorylating the ETS domain-containing protein ELK-1. Phosphorylated ELK-1 subsequently binds to the promoter of the MLCK gene increasing its transcription [16]. However, we did not observe an upregulation of MLCK by DCA indicating that this is not the mechanism causing increased MLC phosphorylation. On the other hand, the activity of MLC phosphatase is regulated by phosphorylation of the MYPT1 regulatory subunit at threonine 696 and 853. This is done by the kinases ERK1/2 and ROCK, leading to the inhibition of MLCP activity [35-37]. DCA increased MYTP phosphorylation which was inhibited by EC and the NADPH oxidase and ERK1/2 inhibitors. This suggests that the inhibition of MLCP is one

mechanism involved in DCA/ ERK1/2-mediated increased levels of phosphorylated MLC in Caco-2 cells, and consequent monolayer permeabilization.

Other adverse effect of bile acids is the downregulation of TJ proteins. In rodents chronically fed a high-fat diet there is a decreased expression of TJ proteins including ZO-1, occludin, claudin-1, claudin-3, and junctional adhesion molecule-1 [11, 20]. Accordingly, bile juice isolated from rats fed a high-fat diet promoted Caco-2 cell monolayer permeabilization and the downregulation of claudin-1, claudin-3, and junctional adhesion molecule-1 [11]. DCA-treated *Apc*$^{min/+}$ mice also show a decreased expression of ZO-1 [38]. We observed that DCA decreased the protein content of ZO-1 and occludin, which was prevented by EC, and both NADPH oxidase and ERK1/2 inhibitors. On the other hand, the EC isomer (+)-catechin did not prevent inflammation-induced decrease in ZO-1 and occludin expression and consequent monolayer permeabilization [39]. This stresses the critical importance of the stereospecificity of flavonoids on their biological actions. Metalloproteinases have been found to be involved in the degradation of TJ proteins [40]. The activation of MMP-9 and MMP-2 was found to be responsible for the low levels of ZO-1, occludin and JAM-A in cholesterol oxidation products-treated Caco-2 cells [41]. Consistently, EC and NADPH oxidase and MEK/ERK inhibitors prevented DCA-mediated MMP-2 activation. Accordingly, ERK1/2 regulates the expression of MMP-2. MEK1 constitutive activation causes increased MMP-2 and MMP-9 activity and decreases ZO-1 and occludin levels in intestinal epithelial cells [42]. Thus, the protection of TJ structure via downregulation of MMP-2 is another mechanism involved in EC-mediated protection against the adverse effects of DCA.

We conclude that bile acids play a central role in high-fat diet-induced intestinal permeabilization. The capacity of EC supplementation to prevent high-fat diet-induced

permeabilization and endotoxemia in mice can be in part explained by its preventive effects on bile acid-induced loss of TJ structure and function. Evidence suggest that EC acts in part preventing NADPH oxidase upregulation, increased oxidant production, and the activation of the redox-sensitive ERK1/2 signaling pathway. Through these mechanisms, diets rich in EC can contribute to protect the gastrointestinal tract from the adverse effects of high fat consumption.

Acknowledgements

This work was supported by H.E. Jastro awards to Z.W., grant NIFA-USDA (CA-D*-xxx-7244-H) to P.O., and by University of East Anglia, Faculty of Medicine and Health Sciences funds attributed to M.M. and D.V. P.O. is a correspondent researcher from CONICET, Argentina.

Author contributions

D.V. and M.M. performed the individual bile acid samples analyses. Z.W. and C.L. ran all other experiments. P.I.O. designed the study and wrote the manuscript. All authors revised the article, critically reviewed it for intellectual content, and approved the final version.

Legend to figures

Figure 1. Effects of a high-fat diet and of EC supplementation on fecal/cecal bile acid profiles in mice. Mice were fed a control diet (empty bars), a high-fat diet (HF) (black bars), or the high-fat diet supplemented with 20 mg EC/kg body weight (HFE) (blue bars). **A**- Total fecal bile acids and **B-E**- individual cecum bile acids were measured as described in methods. Results are shown as means ± SEM and are the average of 5-7 animals/group. Values having different superscripts are significantly different ($p < 0.05$, One-way ANOVA).

MCA: muricholic acid, CA: cholic acid, CDCA: chenodeoxycholic acid, DCA, deoxycholic acid; LCA: lithocholic acid, HDCA: hyodeoxycholic acid, UDCA: ursodeoxycholic acid, T-α-MCA: tauro-α-muricholic acid, T-β-MCA: tauro-β-muricholic acid, TCA: taurocholic acid, TCDCA: taurochenodeoxycholic acid, THCA: taurohyocholic acid, GCA: glycholic acid, GCDCA: glycochenodeoxycholic acid, TDCA: taurodeoxycholic acid, TLC: taurolithocholic acid, THDCA: taurohyodeoxycholic acid, TUDCA: tauroursodeoxycholic acid, GDCA: glycohyodeoxycholic acid and GHDCA: glycohyodeoxycholic acid.

Figure 2. DCA causes an increase in Caco-2 cell monolayer paracellular permeability that is prevented by EC. Caco-2 cell monolayers were treated with 100 µM DCA in the absence or the presence of 0-10 µM EC added to the upper chamber and cells incubated for 0-4 h. Caco-2 cell monolayer permeability was evaluated by measuring FITC-dextran paracellular transport. **A**- Cell viability of Caco-2 cells treated with DCA and in the absence or the presence of 1-10 µM EC for 6 h. **B**- Kinetics of FITC-dextran paracellular transport in Caco-2 monolayers in the absence of additions

(empty circles), and in the presence of 100 µM DCA without (black triangles) or with (blue triangles) simultaneous addition of 5 µM EC. *Significantly different from controls at the corresponding time point. **C,D**- Dose-dependent inhibition by EC of DCA-induced FITC-dextran paracellular transport after 2 h (**C**) or 4 h (**D**) incubation. Results are shown as mean ± SEM of 5 independent experiments. **A,C,D**- Data were normalized to control values. Values having different superscripts are significantly different ($p<0.05$, One-way ANOVA).

Figure 3. DCA causes an increase in Caco-2 cell oxidant: effects of EC. Caco-2 cell monolayers were treated with 100 µM DCA in the absence or the presence of 5 µM EC for 0-4 h. **A,B**- mRNA levels of NOX1 and NOX4 were measured by RT-PCR and referred to β-actin mRNA content. mRNA levels were measured **A**-between 0-4 h for cells incubated without or with DCA, or **B**- for 2 h without or with addition of DCA and in the absence or the presence of 5 µM EC. **C-** Kinetics (0-4 h) of oxidant production evaluated using the probes Amplex® Red (red circles), DCFDA (grey triangles), and DHE (blue triangles) as described in methods. **D-** Effects of DCA and 5 µM EC on oxidant production as measured with Amplex® Red (AR) after 1 h incubation, or with DCFDA and DHE after 4 h incubation. **E-G**- Mitochondrial oxidant production was evaluated with MitoSOX. **E-** typical FACS scan profiles for cells incubated in the absence (C) or the presence of 100 µM DCA (DCA). NC: negative control of cells not added with MitoSOX**. F-** Kinetics of MitoSOX fluorescence of cells incubated in the presence of DCA. **G**- MitoSOX fluorescence in cells incubated without or with DCA and in the absence or presence of 5 µM EC for 2 h. Results are shown as mean ± SEM of 4-5 independent experiments. Data were normalized to control values. Kinetic graphs: control values are shown as a dashed grey line. *Significantly different from controls at the corresponding

time point. Bars: values having different superscripts are significantly different ($p<0.05$, One-way ANOVA).

Figure 4. ERK1/2 activation is involved in DCA-induced Caco-2 cell monolayer permeabilization: inhibitory actions of EC and other NADPH oxidase inhibitors. Caco-2 cell monolayers were incubated for 0-4 h with or without 100 µM DCA in the absence or the presence of 5 µM EC, 1 µM apocynin, 1 µM VAS-2870 or 10 µM U0126. **A-** The kinetics of ERK1/2 and NF-κB activation in the presence of 100 µM DCA was evaluated by Western blot by measuring the phosphorylation of ERK1/2 (T202/Y204) and p65 (Ser536), respectively. **B-** Cells were incubated with or without 100 µM DCA and in the absence or the presence of 1 µM EC for either 0.5 h to assess EGFR phosphorylation (Tyr1068) or 2 h for ERK1/2 phosphorylation. **C,D-** Cells were incubated with or without 100 µM DCA and in the absence or the presence of apocynin, VAS-2870 or U0126 for 2 h. **C,D**- Effects of the NADPH oxidase and ERK1/2 inhibitors on (**C**) DCA-induced ERK1/2 phosphorylation measured by Western blot, and (**D**) Caco-2 cell monolayer permeabilization evaluated as the FITC-dextran paracellular transport. Western blot bands were quantified and values for phosphorylated proteins were referred to the respective total protein content. Results are shown as mean ± SEM of 4-6 independent experiments. **A-** *Significantly different from controls at the corresponding time point. **B-D**- Values having different superscripts are significantly different ($p<0.05$, One-way ANOVA).

Figure 5. DCA promotes an increase in MLC phosphorylation independently from MLCK but dependent on MLC phosphatase inhibition: effects of EC, and NADPH oxidase and ERK1/2

inhibitors. Caco-2 cell monolayers were incubated for 2 h with or without 100 µM DCA and in the absence or the presence of 5 µM EC, 1 µM apocynin, 1 µM VAS-2870 or 10 µM U0126. (**A**) MLC (Ser19) and (**D**) MYPT1 (Thr696) phosphorylation levels were measured by Western blot. After quantification values for phosphorylated proteins were referred to the respective total protein content. β-actin was measured as loading control. **B,C**- MLCK mRNA levels were measured by RT-PCR and values referred to the β-actin mRNA content. **B**- Kinetics of DCA-mediated effects on MLCK mRNA levels, **C**- Effects of the inhibitors on the MLCK mRNA content after 2 h incubation with DCA. Results are shown as mean ± SEM of 4-6 independent experiments. Values having different superscripts are significantly different ($p<0.05$, One-way ANOVA).

Figure 6. DCA decreases the expression of tight junction proteins: effects of EC, NADPH oxidase and ERK1/2 inhibitors. Caco-2 cell monolayers were incubated for 0-4 h with or without 100 µM DCA and in the absence or the presence of 5 µM EC, 1 µM apocynin, 1 µM VAS-2870 or 10 µM U0126. The expression of TJ proteins (ZO-1, occludin, claudin-1 and claudin-2) was measured by Western blot. Bands were quantified and values referred to β-actin levels. **A-**Kinetics of DCA-mediated effects on ZO-1 (full circles), occludin (black triangles), claudin-1 (empty circles) and claudin-2 (red triangles) protein profiles. **B-D-** Effects of EC, apocynin, VAS-2870 and U0126 on occludin (**B**) and ZO-1 (**C**) protein levels and (**D**) MMP-2 activity measured by zymography after 2 h incubation with 100 µM DCA. Results are shown as mean ± SE of 4-6 independent experiments. Values having different superscripts are significantly different ($p<0.05$, One-way ANOVA test).

References

[1] X. He, K. Wu, S. Ogino, E. L. Giovannucci, A. T. Chan, M. Song, Association Between Risk Factors for Colorectal Cancer and Risk of Serrated Polyps and Conventional Adenomas, Gastroenterology. 2 (2018) 355-373 e318.

[2] R. M. Gadaleta, O. Garcia-Irigoyen, A. Moschetta, Bile acids and colon cancer: Is FXR the solution of the conundrum?, Mol. Aspects Med. (2017) 66-74.

[3] A. Damms-Machado, S. Louis, A. Schnitzer, V. Volynets, A. Rings, M. Basrai, S. C. Bischoff, Gut permeability is related to body weight, fatty liver disease, and insulin resistance in obese individuals undergoing weight reduction, Am. J. Clin. Nutr. 1 (2017) 127-135.

[4] F. Siracusa, N. Schaltenberg, E. J. Villablanca, S. Huber, N. Gagliani, Dietary Habits and Intestinal Immunity: From Food Intake to CD4(+) T H Cells, Front Immunol. (2018) 3177.

[5] M. A. Odenwald, J. R. Turner, The intestinal epithelial barrier: a therapeutic target?, Nat. Rev. Gastroenterol Hepatol. 1 (2017) 9-21.

[6] J. Konig, J. Wells, P. D. Cani, C. L. Garcia-Rodenas, T. MacDonald, A. Mercenier, J. Whyte, F. Troost, R. J. Brummer, Human Intestinal Barrier Function in Health and Disease, Clin. Transl. Gastroenterol. 10 (2016) e196.

[7] J. Tomas, C. Mulet, A. Saffarian, J. B. Cavin, R. Ducroc, B. Regnault, C. Kun Tan, K. Duszka, R. Burcelin, W. Wahli, P. J. Sansonetti, T. Pedron, High-fat diet modifies the PPAR-gamma pathway leading to disruption of microbial and physiological ecosystem in murine small intestine, Proc. Natl. Acad. Sci. U S A (2016).

[8] K.-A. Kim, W. Gu, I.-A. Lee, E.-H. Joh, D.-H. Kim, High fat diet-induced gut microbiota exacerbates inflammation and obesity in mice via the TLR4 signaling pathway, PloS one. 10 (2012) e47713.

[9] M. W. Rohr, C. A. Narasimhulu, T. A. Rudeski-Rohr, S. Parthasarathy, Negative Effects of a High-Fat Diet on Intestinal Permeability: A Review, Adv. Nutr. (2019).

[10] A. Buckley, J. R. Turner, Cell Biology of Tight Junction Barrier Regulation and Mucosal Disease, Cold Spring Harb Perspect Biol. 1 (2018).

[11] T. Suzuki, H. Hara, Dietary fat and bile juice, but not obesity, are responsible for the increase in small intestinal permeability induced through the suppression of tight junction protein expression in LETO and OLETF rats, Nutr. Metab. (Lond) (2010) 19.

[12] A. G. Erlejman, C. G. Fraga, P. I. Oteiza, Procyanidins protect Caco-2 cells from bile acid- and oxidant-induced damage, Free Radic. Biol. Med. 8 (2006) 1247-1256.

[13] S. Jean-Louis, S. Akare, M. A. Ali, E. A. Mash, Jr., E. Meuillet, J. D. Martinez, Deoxycholic acid induces intracellular signaling through membrane perturbations, J. Biol. Chem. 21 (2006) 14948-14960.

[14] F. Raimondi, P. Santoro, M. V. Barone, S. Pappacoda, M. L. Barretta, M. Nanayakkara, C. Apicella, L. Capasso, R. Paludetto, Bile acids modulate tight junction structure and barrier function of Caco-2 monolayers via EGFR activation, American Journal of Physiology-Gastrointestinal and Liver Physiology. 4 (2008) G906-G913.

[15] M. Da Silva, G. K. Jaggers, S. V. Verstraeten, A. G. Erlejman, C. G. Fraga, P. I. Oteiza, Large procyanidins prevent bile-acid-induced oxidant production and membrane-initiated ERK1/2, p38, and Akt activation in Caco-2 cells, Free Radic. Biol. Med. 1 (2012) 151-159.

[16] R. Al-Sadi, S. Guo, D. Ye, T. Y. Ma, TNF-alpha modulation of intestinal epithelial tight junction barrier is regulated by ERK1/2 activation of Elk-1, Am. J. Pathol. 6 (2013) 1871-1884.

[17] D. Ye, T. Y. Ma, Cellular and molecular mechanisms that mediate basal and tumour necrosis factor-alpha-induced regulation of myosin light chain kinase gene activity, J. Cell Mol. Med. 4 (2008) 1331-1346.
[18] P. I. Oteiza, C. G. Fraga, D. A. Mills, D. H. Taft, Flavonoids and the gastrointestinal tract: Local and systemic effects, Mol. Aspects Med. (2018).
[19] T. C. Contreras, E. Ricciardi, E. Cremonini, P. I. Oteiza, (-)-Epicatechin in the prevention of tumor necrosis alpha-induced loss of Caco-2 cell barrier integrity, Arch. Biochem. Biophys. (2015) 84-91.
[20] E. Cremonini, Z. Wang, A. Bettaieb, A. M. Adamo, E. Daveri, D. A. Mills, K. M. Kalanetra, F. G. Haj, S. Karakas, P. I. Oteiza, (-)-Epicatechin protects the intestinal barrier from high fat diet-induced permeabilization: Implications for steatosis and insulin resistance, Redox Biol. (2018) 588-599.
[21] J. de Wael, C. E. Raaymakers, H. J. Endeman, Simplified quantitative determination of total fecal bile acids, Clin. Chim. Acta. 2 (1977) 465-470.
[22] J. L. Porter, J. S. Fordtran, C. A. Santa Ana, M. Emmett, L. R. Hagey, E. A. Macdonald, A. F. Hofmann, Accurate enzymatic measurement of fecal bile acids in patients with malabsorption, J. Lab. Clin. Med. 6 (2003) 411-418.
[23] M. M. Bradford, A rapid and sensitive method for the quantitation of microgram quantities of protein utilizing the principle of protein-dye binding, Anal. Biochem. (1976) 248-254.
[24] Y. Murakami, S. Tanabe, T. Suzuki, High-fat Diet-induced Intestinal Hyperpermeability is Associated with Increased Bile Acids in the Large Intestine of Mice, J. Food Sci. 1 (2016) H216-222.
[25] S. L. Long, C. G. M. Gahan, S. A. Joyce, Interactions between gut bacteria and bile in health and disease, Mol. Aspects Med. (2017) 54-65.
[26] A. P. Moreira, T. F. Texeira, A. B. Ferreira, C. Peluzio Mdo, C. Alfenas Rde, Influence of a high-fat diet on gut microbiota, intestinal permeability and metabolic endotoxaemia, Br. J. Nutr. 5 (2012) 801-809.
[27] P. D. Cani, J. Amar, M. A. Iglesias, M. Poggi, C. Knauf, D. Bastelica, A. M. Neyrinck, F. Fava, K. M. Tuohy, C. Chabo, A. Waget, E. Delmee, B. Cousin, T. Sulpice, B. Chamontin, J. Ferrieres, J. F. Tanti, G. R. Gibson, L. Casteilla, N. M. Delzenne, M. C. Alessi, R. Burcelin, Metabolic endotoxemia initiates obesity and insulin resistance, Diabetes. 7 (2007) 1761-1772.
[28] N. Ohtani, S. Yoshimoto, E. Hara, Obesity and cancer: a gut microbial connection, Cancer Res. 7 (2014) 1885-1889.
[29] Y. Sambuy, I. De Angelis, G. Ranaldi, M. L. Scarino, A. Stammati, F. Zucco, The Caco-2 cell line as a model of the intestinal barrier: influence of cell and culture-related factors on Caco-2 cell functional characteristics, Cell Biol. Toxicol. 1 (2005) 1-26.
[30] Y. Steffen, C. Gruber, T. Schewe, H. Sies, Mono-O-methylated flavanols and other flavonoids as inhibitors of endothelial NADPH oxidase, Arch. Biochem. Biophys. 2 (2008) 209-219.
[31] K. Allen, N. D. Kim, J. O. Moon, B. L. Copple, Upregulation of early growth response factor-1 by bile acids requires mitogen-activated protein kinase signaling, Toxicol. Appl. Pharmacol. 1 (2010) 63-67.
[32] Y. P. Rao, E. J. Studer, R. T. Stravitz, S. Gupta, L. Qiao, P. Dent, P. B. Hylemon, Activation of the Raf-1/MEK/ERK cascade by bile acids occurs via the epidermal growth factor receptor in primary rat hepatocytes, Hepatology. 2 (2002) 307-314.
[33] C. M. Payne, C. Weber, C. Crowley-Skillicorn, K. Dvorak, H. Bernstein, C. Bernstein, H. Holubec, B. Dvorakova, H. Garewal, Deoxycholate induces mitochondrial oxidative stress and activates NF-kappaB through multiple mechanisms in HCT-116 colon epithelial cells, Carcinogenesis. 1 (2007) 215-222.
[34] Y. Araki, T. Katoh, A. Ogawa, S. Bamba, A. Andoh, S. Koyama, Y. Fujiyama, T. Bamba, Bile acid modulates transepithelial permeability via the generation of reactive oxygen species in the Caco-2 cell line, Free Radic. Biol. Med. 6 (2005) 769-780.

[35] D. Xiao, L. D. Longo, L. Zhang, Alpha1-adrenoceptor-mediated phosphorylation of MYPT-1 and CPI-17 in the uterine artery: role of ERK/PKC, Am. J. Physiol. Heart Circ. Physiol. 6 (2005) H2828-2835.
[36] M. E. Grassie, L. D. Moffat, M. P. Walsh, J. A. MacDonald, The myosin phosphatase targeting protein (MYPT) family: a regulated mechanism for achieving substrate specificity of the catalytic subunit of protein phosphatase type 1delta, Arch. Biochem. Biophys. 2 (2011) 147-159.
[37] E. Ihara, Q. Yu, M. Chappellaz, J. A. MacDonald, ERK and p38MAPK pathways regulate myosin light chain phosphatase and contribute to Ca2+ sensitization of intestinal smooth muscle contraction, Neurogastroenterol Motil. 1 (2015) 135-146.
[38] L. Liu, W. Dong, S. Wang, Y. Zhang, T. Liu, R. Xie, B. Wang, H. Cao, Deoxycholic acid disrupts the intestinal mucosal barrier and promotes intestinal tumorigenesis, Food Funct. 11 (2018) 5588-5597.
[39] M. G. Bianchi, M. Chiu, G. Taurino, F. Brighenti, D. Del Rio, P. Mena, O. Bussolati, Catechin and Procyanidin B2 Modulate the Expression of Tight Junction Proteins but Do Not Protect from Inflammation-Induced Changes in Permeability in Human Intestinal Cell Monolayers, Nutrients. 10 (2019).
[40] K. R. Groschwitz, D. Wu, H. Osterfeld, R. Ahrens, S. P. Hogan, Chymase-mediated intestinal epithelial permeability is regulated by a protease-activating receptor/matrix metalloproteinase-2-dependent mechanism, Am. J. Physiol. Gastrointest Liver Physiol. 5 (2013) G479-489.
[41] M. Deiana, S. Calfapietra, A. Incani, A. Atzeri, D. Rossin, R. Loi, B. Sottero, N. Iaia, G. Poli, F. Biasi, Derangement of intestinal epithelial cell monolayer by dietary cholesterol oxidation products, Free Radic. Biol. Med. (2017) 539-550.
[42] E. Lemieux, S. Bergeron, V. Durand, C. Asselin, C. Saucier, N. Rivard, Constitutively active MEK1 is sufficient to induce epithelial-to-mesenchymal transition in intestinal epithelial cells and to promote tumor invasion and metastasis, Int. J. Cancer. 7 (2009) 1575-1586.

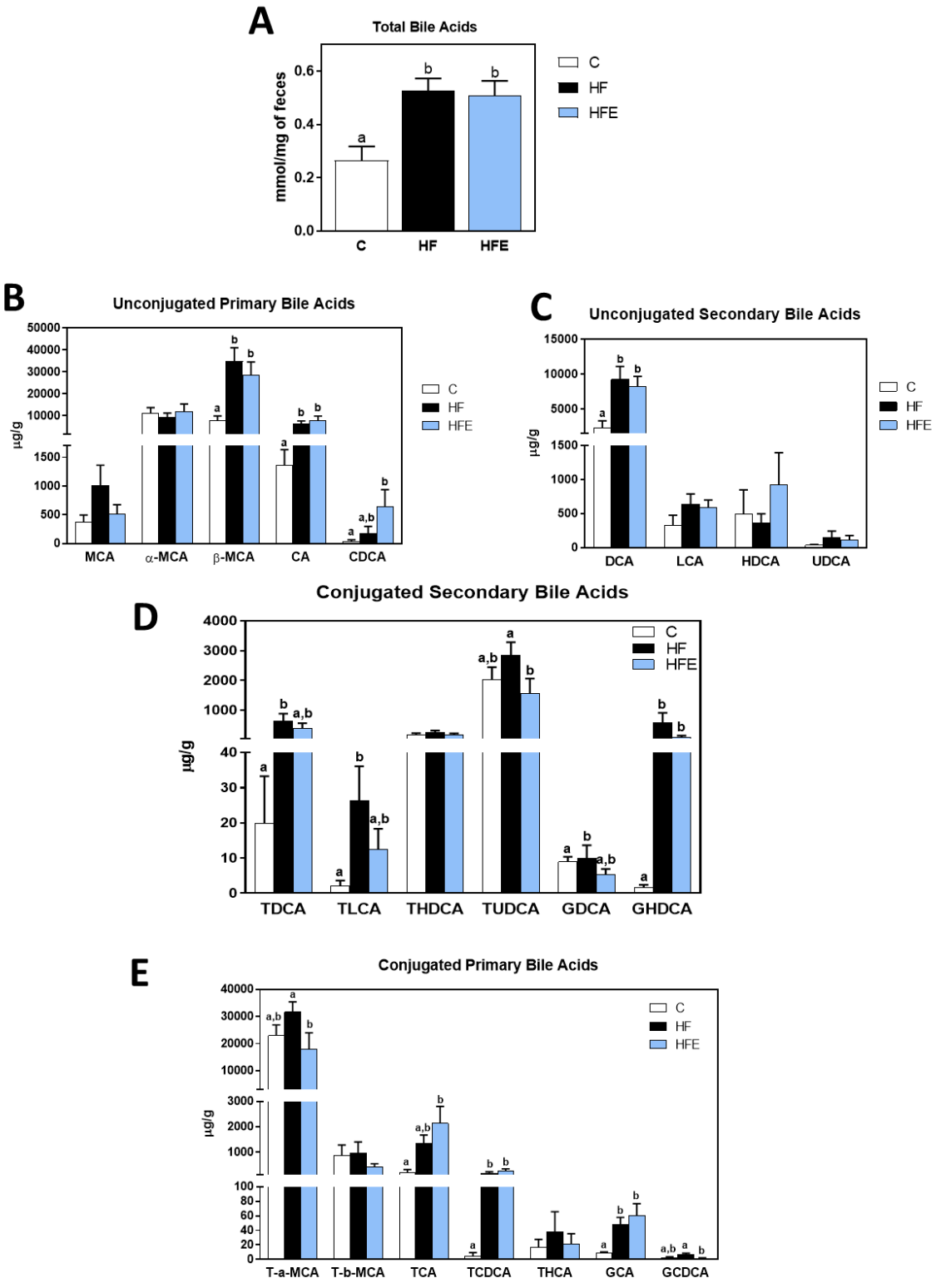
A
Total Bile Acids
mmol/mg of feces
C
HF
HFE
B
Unconjugated Primary Bile Acids
μg/g
MCA
α-MCA
β-MCA
CA
CDCA
C
Unconjugated Secondary Bile Acids
DCA
LCA
HDCA
UDCA
D
Conjugated Secondary Bile Acids
TDCA
TLCA
THDCA
TUDCA
GDCA
GHDCA
E
Conjugated Primary Bile Acids
T-a-MCA
T-b-MCA
TCA
TCDCA
THCA
GCA
GCDCA

Figure 1

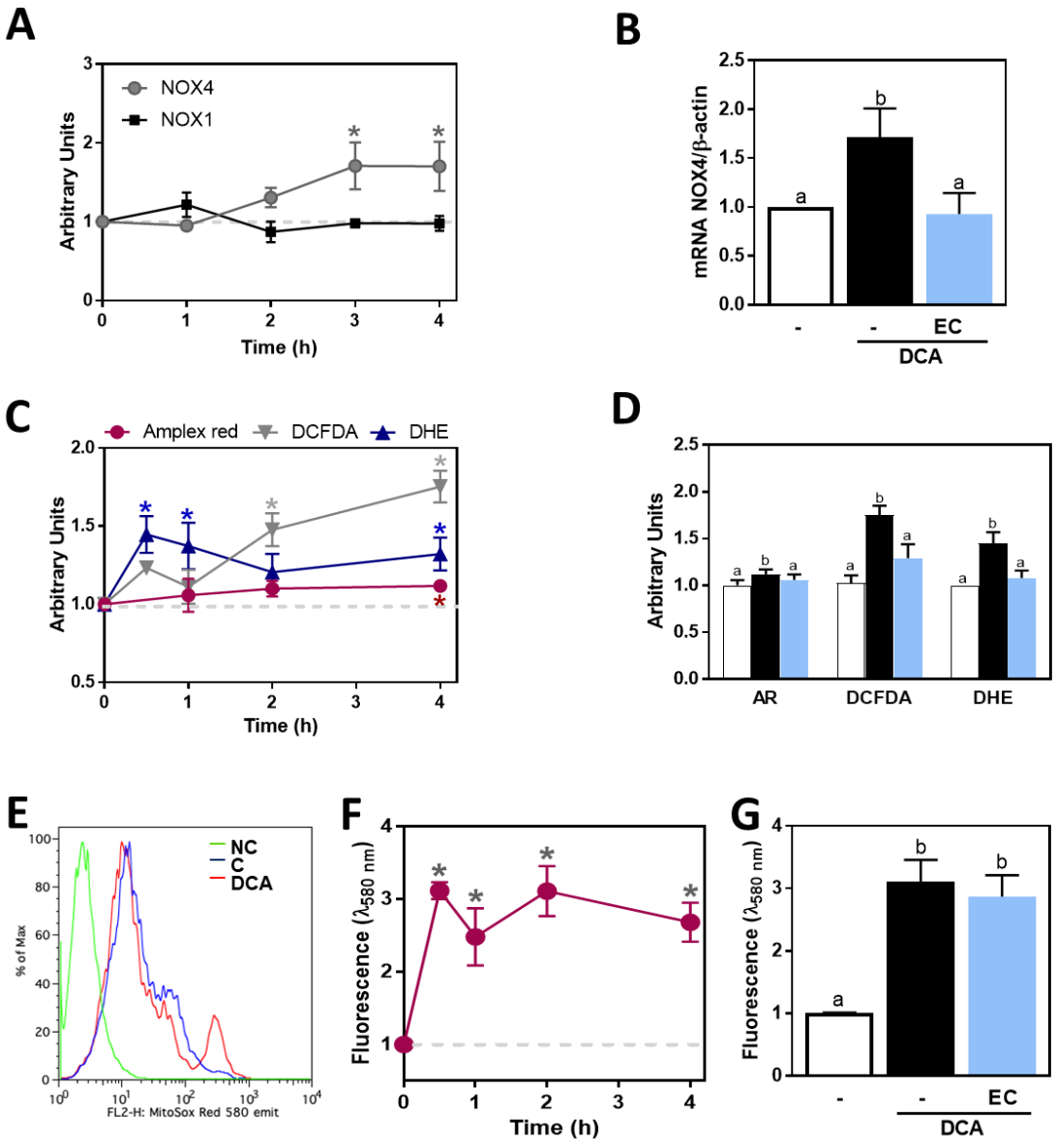
A
NOX4
NOX1
Arbitrary Units
Time (h)
B
mRNA NOX4/β-actin
a
b
a
-
-
EC
DCA
C
Amplex red
DCFDA
DHE
Arbitrary Units
Time (h)
D
Arbitrary Units
AR
DCFDA
DHE
E
NC
C
DCA
% of Max
FL2-H: MitoSox Red 580 emit
F
Fluorescence (λ580 nm)
Time (h)
G
Fluorescence (λ580 nm)
a
b
b
-
-
EC
DCA

Figure 3

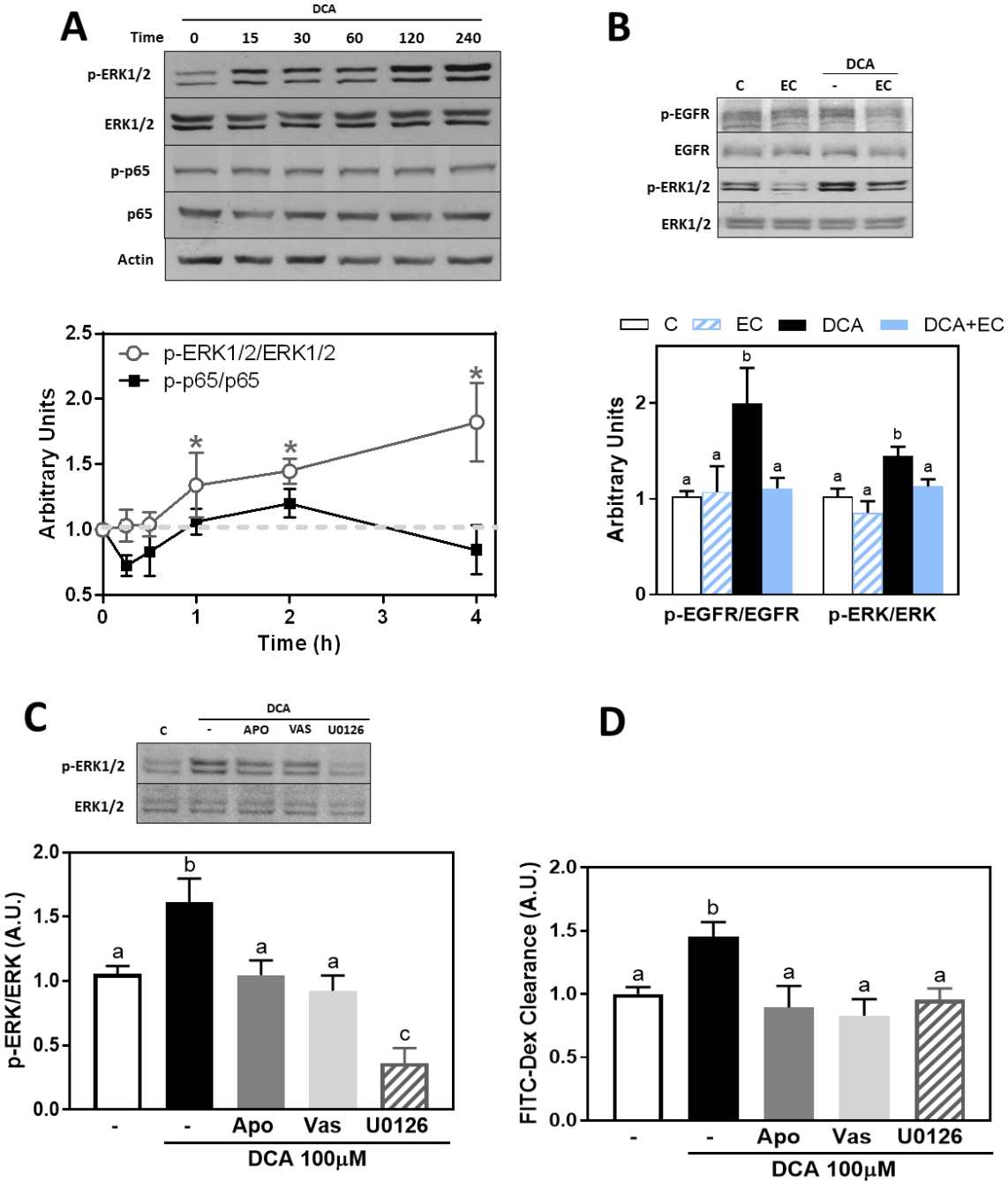
A
DCA
Time 0 15 30 60 120 240
p-ERK1/2
ERK1/2
p-p65
p65
Actin
p-ERK1/2/ERK1/2
p-p65/p65
Arbitrary Units
Time (h)
B
DCA
C EC - EC
p-EGFR
EGFR
p-ERK1/2
ERK1/2
C EC DCA DCA+EC
Arbitrary Units
p-EGFR/EGFR
p-ERK/ERK
C
DCA
C - APO VAS U0126
p-ERK1/2
ERK1/2
p-ERK/ERK (A.U.)
- - Apo Vas U0126
DCA 100μM
D
FITC-Dex Clearance (A.U.)
- - Apo Vas U0126
DCA 100μM

Figure 4

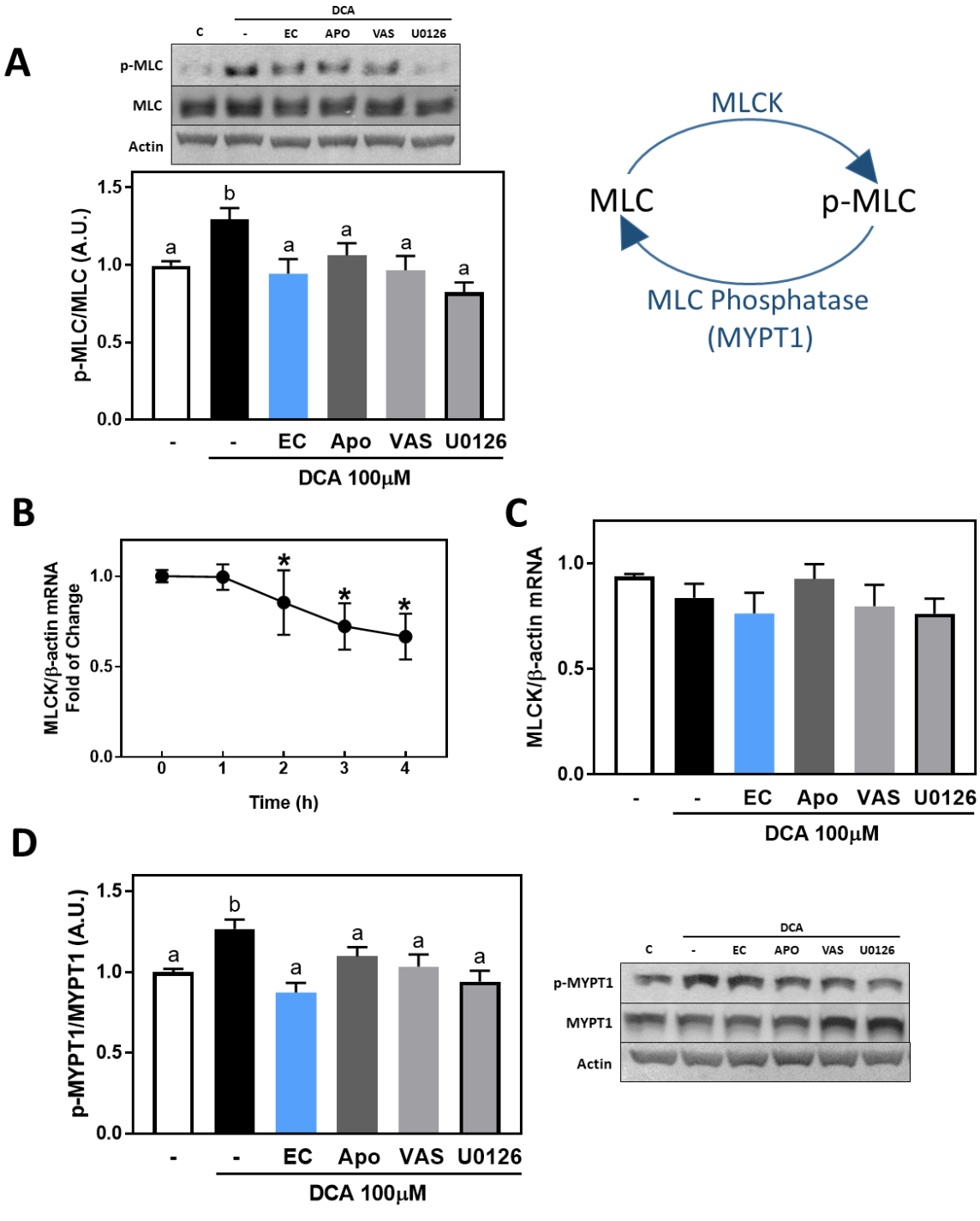
A
DCA
C
-
EC
APO
VAS
U0126
p-MLC
MLC
Actin
p-MLC/MLC (A.U.)
1.5
1.0
0.5
0.0
a
b
a
a
a
a
-
-
EC
Apo
VAS
U0126
DCA 100μM
MLCK
MLC
p-MLC
MLC Phosphatase
(MYPT1)
B
MLCK/β-actin mRNA
Fold of Change
1.0
0.5
0.0
*
*
*
0
1
2
3
4
Time (h)
C
MLCK/β-actin mRNA
1.0
0.5
0.0
-
-
EC
Apo
VAS
U0126
DCA 100μM
D
p-MYPT1/MYPT1 (A.U.)
1.5
1.0
0.5
0.0
a
b
a
a
a
a
-
-
EC
Apo
VAS
U0126
DCA 100μM
DCA
C
-
EC
APO
VAS
U0126
p-MYPT1
MYPT1
Actin

Figure 5

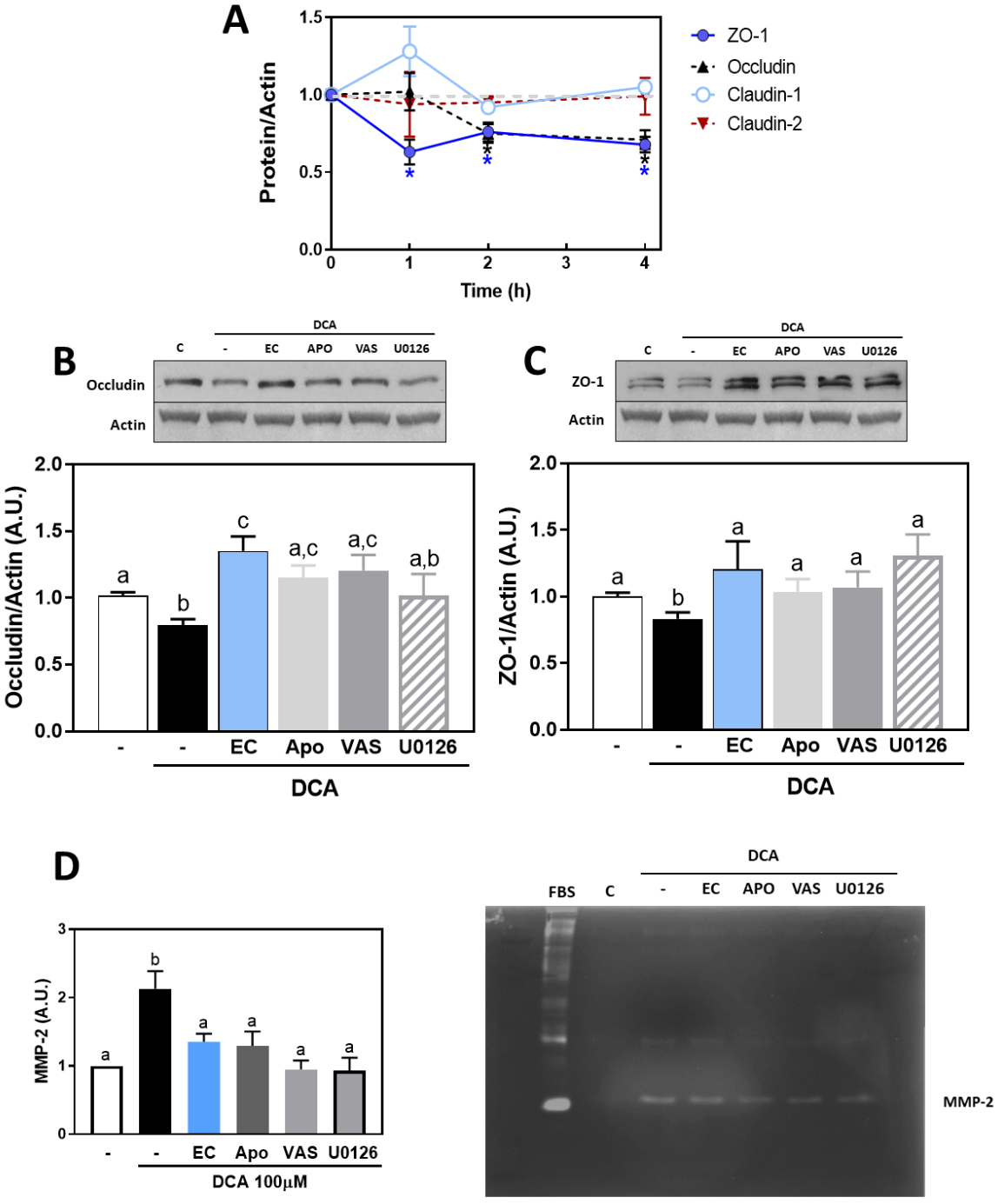
A
Protein/Actin
Time (h)
ZO-1
Occludin
Claudin-1
Claudin-2
B
Occludin
Actin
C
ZO-1
Actin
DCA
C
-
EC
APO
VAS
U0126
Occludin/Actin (A.U.)
ZO-1/Actin (A.U.)
Apo
D
MMP-2 (A.U.)
DCA 100μM
FBS
MMP-2

Figure 6

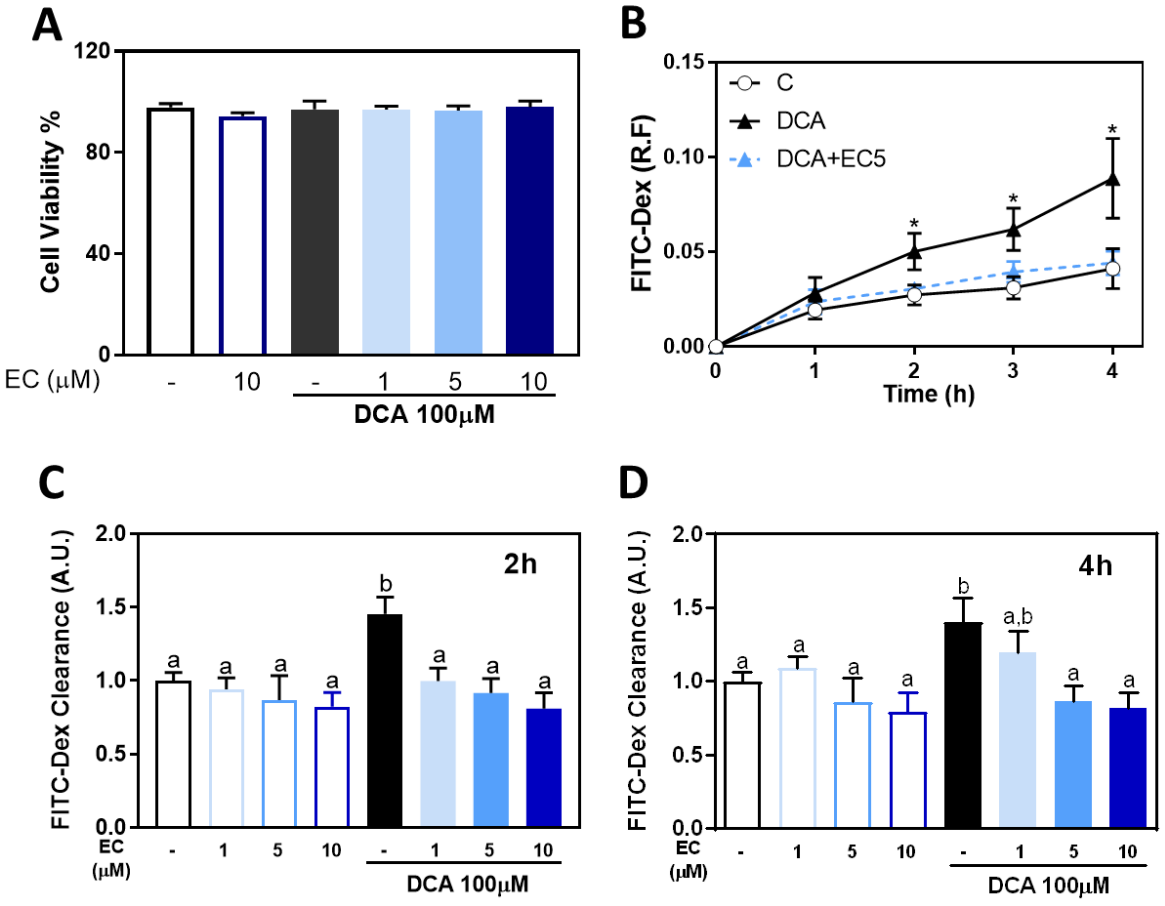
A
Cell Viability %
120
80
40
0
EC (μM)
-
10
-
1
5
10
DCA 100μM
B
FITC-Dex (R.F)
0.15
0.10
0.05
0.00
C
DCA
DCA+EC5
0
1
2
3
4
Time (h)
C
FITC-Dex Clearance (A.U.)
2.0
1.5
1.0
0.5
0.0
2h
a
a
a
a
b
a
a
a
EC (μM)
-
1
5
10
-
1
5
10
DCA 100μM
D
FITC-Dex Clearance (A.U.)
4h
a
a
a
a
b
a,b
a
a
DCA 100μM

Figure 2

Conflict of Interest

None of the authors has any activity that represents a conflict of interest with this work.